MOX–Report No. 15/2008

An anisotropic mesh adaptation procedure for an optimal control problem of the advection-diffusion-reaction equation

Stefano Micheletti, Simona Perotto

MOX, Dipartimento di Matematica "F. Brioschi"
Politecnico di Milano, Via Bonardi 29 - 20133 Milano (Italy)

mox@mate.polimi.it http://mox.polimi.it

An anisotropic mesh adaptation procedure for an optimal control problem of the advection-diffusion-reaction equation *

Stefano Micheletti and Simona Perotto[♯]

17 June 2008

[♯] MOX– Modellistica e Calcolo Scientifico
Dipartimento di Matematica "F. Brioschi"
Politecnico di Milano
via Bonardi 9, 20133 Milano, Italy
{stefano.micheletti,simona.perotto}@polimi.it

Keywords: anisotropic mesh adaptation, optimal control, advection-diffusion-reaction equation, finite elements

AMS Subject Classification: 65N15, 65N30, 65N50, 65K10

Abstract

We derive an anisotropic a posteriori error estimator for a PDE-constrained optimal control problem, governed by the scalar advection-diffusion-reaction equation. With a view to the advection dominated case, a strongly consistent symmetric stabilization is employed so that the "optimize-then-discretize" and "discretize-then-optimize" philosophies coincide and lead to the same discrete problem. The estimator is turned into an anisotropic mesh adaptation procedure which allows us to approximate the cost functional within to a given tolerance. Both an academic and a realistic test, inspired by an environmental application, assess the performance of the proposed approach.

1 Introduction and motivations

Optimal control problems are likely the most interesting in science and engineering, where they raise a lot of challenges. In any manufacturing or design

*This research was supported by COFIN 2006 "Metodi Numerici Avanzati per il Calcolo Scientifico".

process there is always, sooner or later, a phase where some optimization process is required. For instance, a race car in Formula 1 should contain the consumed fuel while minimizing the lap time by a suitable race strategy (instantaneous velocity, number of pit-stops, etc), adapted to the characteristics of a given circuit and the unpredictable race situations; in swimming races, the swimmer should optimize his/her stroke while undertaking the least physical effort; in microelectronics, a given semiconductor device must be designed (for example, by acting on its doping profile) so as to limit power consumption while maximizing some performance index (e.g., the switching speed); in medical surgery, the shape of a by-pass has to be optimized to reduce the vorticity downstream the graft, responsible of a possible new stenosys; in environmental issues, the concentration of toxic substances and pollutants emitted by industrial plants near a town (rather than of contaminants dumped in a river) should be kept below some attention level, without compromising the production rate of the factories involved.

In all these applications the specific objective can actually be formalized via a suitable optimal control problem, in terms of the minimization of a suitable cost functional. This typically involves the discrepancy between the quantity to be controlled and a given observation. On the other hand the physical problem under investigation can be often modeled by partial differential equations (PDE's), typically translating the space/time conservation of the main quantities involved in the process. These equations play the role of a constraint to the optimal control problem, depending on the state (the quantity to be controlled) and the control (the quantity acting as regulator). To conclude with, we are dealing with PDE-constrained optimal control problems ([3]).

In this paper we focus on a model optimal control problem: the governing equation is an elliptic PDE, namely, the scalar advection-diffusion-reaction equation. The considered setting is fairly simple, i.e., both the observation and the control are distributed and fully homogeneous Dirichlet boundary conditions are enforced. We are primarily concerned with the numerical approximation of this optimal control problem through a Galerkin method employing continuous piecewise affine finite elements. Our actual aim is the derivation of an a posteriori error estimator able to drive a suitable mesh adaptation procedure with a view to advection dominated problems. As a matter of fact it is well known that, in such a case, the physical solution often exhibits strong directional features (e.g., boundary or internal layers), where the numerical approximation may show spurious oscillations on a mesh which is not sufficiently fine. A convenient stabilization scheme combined with a mesh adaptation procedure is a standard remedy to this matter. This raises a long-debated issue in the literature ([16, 2, 5, 1, 11, 14]). Two reciprocal approaches are indeed pursued: the so-called "optimize-then-discretize" philosophy versus the "discretize-then-optimize" strategy. So far, none of these two has been definitely shown to better-off the other. There are cases where the first approach performs better, while in other circumstances it fails ([16]). As highlighted in [5], a possible remedy to this dilemma is the employment of a symmetric and strongly consistent sta-

bilization: this makes the two approaches identical and yields also a symmetric discrete optimality system whose solution exhibits optimal convergence rate. We stick to this evidence in choosing the discretization scheme, based on a variant of the strongly-consistent edge-based stabilization proposed by J. Douglas and T. Dupont in [15].

The novelty of the proposed a posteriori error estimator is its capability to detect the directional features of the solution. At each iteration, our adaptive procedure yields a mesh whose elements are not only crowded around the layers but also automatically match the actual directionalities of the solution by a proper sizing, shaping and orientation of the triangles. The more flexibility of an anisotropic adaptation, with respect to the standard isotropic one, where only the size of the triangles is tuned, is a strength point of the proposed methodology in the context of optimal control problems.
To our knowledge, the only paper dealing with anisotropic mesh adaptation in an optimal control setting is [32]. In this paper the author derives an anisotropic a posteriori error estimator for the heat equation. However, no mesh adaptation procedure is devised. Moreover the purely diffusive nature of the heat equation relieves the author from the embarrassing interplay between discretization and optimization.

The paper is organized as follows. Section 2 presents the model problem along with its discretization, while unraveling the "optimize-then-discretize" versus "discretize-then-optimize" dilemma. In section 3 we introduce the grounds of the reference anisotropic setting. We also derive a new anisotropic estimate to control a directional derivative along a triangle edge, instrumental for the edge-based stabilization scheme. The anisotropic a posteriori error estimator is provided in section 4. This estimator is then converted into an effective anisotropic mesh adaptation procedure as detailed in section 5. Section 6 gathers the results of the numerical assessment, which deals with a benchmark problem and with a test of possible interest in environmental applications. This last test case allows us to check the proposed procedure on a more general framework including Neumann boundary conditions and localized control and observation.

2 The model problem

In this section we introduce the model problem we are interested in, i.e., the standard scalar advection-diffusion-reaction equation

$$\begin{cases} -\nabla \cdot (\varepsilon \nabla u) + \boldsymbol{\beta} \cdot \nabla u + \sigma u = f + q & \text{in } \Omega \\ u = 0 & \text{on } \partial\Omega, \end{cases} \tag{1}$$

where $\Omega \subset \mathbb{R}^2$ is a bounded polygonal domain with boundary $\partial\Omega$, while the source $f \in L^2(\Omega)$, the control variable $q \in L^2(\Omega)$, the diffusivity $\varepsilon \in L^\infty(\Omega)$, with $\varepsilon \geq \varepsilon_0 > 0$ a.e. in Ω, the reaction $\sigma \in L^\infty(\Omega)$, and the advective field

$\boldsymbol{\beta} \in [L^\infty(\Omega)]^2$, with $\nabla \cdot \boldsymbol{\beta} \in L^\infty(\Omega)$ and $-\frac{1}{2}\nabla \cdot \boldsymbol{\beta} + \sigma \geq 0$ a.e. in Ω, are assigned functions.
Throughout the paper, we use the standard notation to denote the Lebesgue and Sobolev function spaces ([25]). In particular, let ω be a given Lebesgue measurable set in $\mathbb{R}^d$, with $d = 1, 2$, with measure $|\omega|$. Thus $L^\infty(\omega)$ stands for the space of the functions bounded a.e. in ω; $W^{1,\infty}(\omega)$ denotes the space of functions in $L^\infty(\omega)$ whose first order (partial) derivatives belong to $L^\infty(\omega)$; $L^2(\omega)$ is the space of the functions Lebesgue square-integrable, with corresponding norm $\|\cdot\|_{L^2(\omega)}$; $H^k(\omega)$ denotes the space of functions in $L^2(\omega)$ for which the distributional derivatives of order up to $k \geq 1$ belong to $L^2(\omega)$. Moreover let $H_{div}(\omega)$ be the space of vector-valued functions in $[L^2(\omega)]^2$ and with divergence in $L^2(\omega)$ ([6]).

The weak formulation of (1) is provided by

$$\text{find } u \in V \equiv H_0^1(\Omega) \ : \ a(u,\mu) = (f,\mu) + b(q,\mu) \quad \forall \mu \in V, \tag{2}$$

where $(\cdot,\cdot)$ denotes the L^2-scalar product on Ω, $H_0^1(\Omega) = \{v \in H^1(\Omega) \ : \ v\big|_{\partial\Omega} = 0\}$, while the bilinear forms $a(\cdot,\cdot)$ and $b(\cdot,\cdot)$ are given by

$$a(u,\mu) = \int_\Omega \varepsilon \nabla u \cdot \nabla \mu \, d\Omega + \int_\Omega \boldsymbol{\beta} \cdot \nabla u \, \mu \, d\Omega + \int_\Omega \sigma u \, \mu \, d\Omega \quad \forall u, \mu \in V,$$

$$b(q,\mu) = \int_\Omega q \, \mu \, d\Omega \quad \forall \mu \in V.$$

Existence and uniqueness of the solution to (2) follow from the above hypotheses on the problem data ([31]).

With a view to the optimal control problem we have in mind, let Q and H be the space of the controls and of the observations, respectively. Let $J : V \times Q \to \mathbb{R}$ be the cost functional to be minimized. Accordingly to the theory in [24, 3, 5], we pick

$$J(u,q) = \frac{1}{2}\|cu - c_0\|_H^2 + \frac{1}{2}n(q,q), \tag{3}$$

with $c : V \to H$ a linear bounded observation operator; $c_0 \in H$ the observation; $n : Q \times Q \to \mathbb{R}$ a bilinear symmetric and coercive form representing the Tikhonov regularization, with $Q = L^2(\Omega)$. Thus the existence of a unique solution to the optimal control problem

$$\text{minimize} \ \ J(u,q), \ \ \text{with } u \in V \text{ and } \ q \in Q, \ \ \text{subject to } \ (1) \tag{4}$$

is guaranteed (see, e.g., [24]). With a view to the resolution of problem (4) via an "optimize-then-discretize" approach, we introduce the Lagrangian functional

$$\mathcal{L}(u,\lambda,q) = J(u,q) + a(u,\lambda) - b(q,\lambda) - (f,\lambda),$$

where $\lambda \in V$ is the so-called Lagrangian multiplier.
The Euler-Lagrange equations representing the necessary condition for optimality are identified by equality

$$\nabla \mathcal{L}(u, \lambda, q)(v, \mu, r) = 0 \quad \forall \{v, \mu, r\} \in V \times V \times Q,$$

i.e., by the system of equations

$$\mathcal{L}_\lambda(u, \lambda, q)(\mu) = a(u, \mu) - b(q, \mu) - (f, \mu) = 0 \quad \forall \mu \in V,$$

$$\mathcal{L}_u(u, \lambda, q)(v) = a(v, \lambda) + (cu - c_0, cv) = 0 \quad \forall v \in V,$$

$$\mathcal{L}_q(u, \lambda, q)(r) = -b(r, \lambda) + n(q, r) = 0 \quad \forall r \in Q.$$

This is equivalent to solving the problem: find $\{u, \lambda, q\} \in V \times V \times Q$ s.t.

$$\begin{aligned} a(u, \mu) &= b(q, \mu) + (f, \mu) \quad \forall \mu \in V, \\ a(v, \lambda) &= (c_0 - cu, cv) \quad \forall v \in V, \\ n(q, r) &= b(r, \lambda) \quad \forall r \in Q. \end{aligned} \tag{5}$$

The first coincides with the state equation (2); the second is the corresponding adjoint state equation, while the last one is the gradient equation.

As we are interested in applications where advection dominates over diffusion and reaction, a suitable discretization scheme has to be employed to contain the spurious oscillations of the numerical solution.
We adopt a variant of the strongly-consistent edge-based stabilization proposed by J. Douglas and T. Dupont in [15] (see, also, [7, 8]). The choice made for this stabilization scheme is aimed at getting rid of the dilemma "optimize-then-discretize" versus "discretize-then-optimize". Indeed, as observed in [5, 35], the employment of a symmetric stabilization guarantees the commutativity of the optimize and discretize steps. Moreover, as highlighted in [5], such a scheme yields a symmetric discrete optimality system and optimal convergence rate.

Let $\{\mathcal{T}_h\}_h$ be a family of conforming decompositions of $\overline{\Omega}$ into triangles K of diameter h_K ([9]). Let $Q_h = \{v_h \in C^0(\overline{\Omega}) : v_h|_K \in \mathbb{P}_1, \forall K \in \mathcal{T}_h\} \subset Q$ (and subset also of V) denote the subspace of piecewise affine functions, with $\mathbb{P}_1 = \text{span}\{1, x_1, x_2\}$ the space of polynomials of (global) degree less than or equal to one, and let $V_h = Q_h \cap V$.
Thus the adopted discrete counterpart of (5) is given by: find $\{u_h, \lambda_h, q_h\} \in V_h \times V_h \times Q_h$, s.t., $\forall \{\mu_h, v_h, r_h\} \in V_h \times V_h \times Q_h$,

$$a(u_h, \mu_h) + \frac{1}{2} \sum_{K \in \mathcal{T}_h} \left\{ \sum_{e \in \partial K} \int_e \gamma \, h_e^2 \, [\nabla u_h \cdot \mathbf{n}]_e \, [\nabla \mu_h \cdot \mathbf{n}]_e \, ds \right\} = b(q_h, \mu_h) + (f, \mu_h); \tag{6}$$

$$a(v_h, \lambda_h) + \frac{1}{2} \sum_{K \in \mathcal{T}_h} \left\{ \sum_{e \in \partial K} \int_e \gamma \, h_e^2 \, [\nabla \lambda_h \cdot \mathbf{n}]_e \, [\nabla v_h \cdot \mathbf{n}]_e \, ds \right\} = (c_0 - cu_h, cv_h); \tag{7}$$

$$n(q_h, r_h) = b(r_h, \lambda_h), \tag{8}$$

where h_e denotes the length of the edge $e \in \partial K$; $\gamma \in L^\infty(e)$, for any $e \in \mathcal{E}_h \backslash \partial\Omega$, with $\mathcal{E}_h$ the skeleton associated with $\mathcal{T}_h$; $[\cdot]_e$ stands for the jump across the edge e, for any $e \in \mathcal{E}_h \backslash \partial\Omega$, $[\cdot]_e$ vanishing when $e \in \partial\Omega$.

Concerning the stabilization parameter γ in (6)-(7), we follow the recipe

$$\gamma = \gamma_0 \, \min\left\{ \frac{\|\boldsymbol{\beta}\|_2 \, h_e}{2\varepsilon}, 1 \right\} |\boldsymbol{\beta} \cdot \mathbf{n}|, \tag{9}$$

γ_0 being a tuning parameter, and where $\| \cdot \|_2$ denotes the Euclidean norm. Function γ is a variant to the choice made in [8], apparently more suitable when handling anisotropic grids. Also the employment of h_e in (6)-(7) and in (9) instead of h_K, as in [8], is suggested by its more anisotropic feature.

Remark 2.1 *The strong consistency of (6) and (7) leads to add suitable regularity assumptions on the diffusion coefficient, i.e., $\varepsilon \in W^{1,\infty}(\Omega)$. Indeed the jump term $[\nabla u \cdot \mathbf{n}]_e$ vanishes identically when $\nabla u \in H_{div}(\Omega)$ ([6]). Actually the weak formulation $(5)_1$ guarantees that $\varepsilon \nabla u \in H_{div}(\Omega)$. Thus the hypothesis on ε implies $\nabla u \in H_{div}(\Omega)$. This regularity will be assumed henceforth.*

We observe that the "discretize-then-optimize" approach stems from the optimality condition

$$\nabla \mathcal{L}_{stab}(u_h, \lambda_h, q_h)(v_h, \mu_h, r_h) = 0 \quad \forall \{v_h, \mu_h, r_h\} \in V_h \times V_h \times Q_h, \tag{10}$$

which returns (6)-(8), where the stabilized Lagrangian $\mathcal{L}_{stab} : V \times V \times Q \to \mathbb{R}$ is given by

$$\begin{aligned} \mathcal{L}_{stab}(u, \lambda, q) &= J(u, q) + a(u, \lambda) - b(q, \lambda) - (f, \lambda) \\ &+ \frac{1}{2} \sum_{K \in \mathcal{T}_h} \left\{ \sum_{e \in \partial K} \int_e \gamma \, h_e^2 \, [\nabla u \cdot \mathbf{n}]_e \, [\nabla \lambda \cdot \mathbf{n}]_e \, ds \right\}. \end{aligned} \tag{11}$$

Moreover, following Remark 2.1, i.e., thanks to the strongly consistent stabilization, it holds that

$$\nabla \mathcal{L}_{stab}(u, \lambda, q)(v, \mu, r) = \nabla \mathcal{L}(u, \lambda, q)(v, \mu, r) = 0 \quad \forall \{v, \mu, r\} \in V \times V \times Q. \tag{12}$$

By suitably subtracting (10) from (12) (with $\{v, \mu, r\} = \{v_h, \mu_h, r_h\} \in V_h \times V_h \times Q_h$), we obtain the orthogonality relation

$$\nabla \mathcal{L}_{stab}(u, \lambda, q)(v_h, \mu_h, r_h) - \nabla \mathcal{L}_{stab}(u_h, \lambda_h, q_h)(v_h, \mu_h, r_h) = 0$$

for any $\{v_h, \mu_h, r_h\} \in V_h \times V_h \times Q_h$ or, equivalently, as $\mathcal{L}_{stab}$ is quadratic,

$$\nabla^2 \mathcal{L}_{stab}(\cdot, \{u - u_h, \lambda - \lambda_h, q - q_h\}, \{v_h, \mu_h, r_h\}) = 0 \quad \forall \{v_h, \mu_h, r_h\} \in V_h \times V_h \times Q_h.$$

3 The anisotropic framework

We introduce the anisotropic setting used to enrich the a posteriori optimal control analysis with directional information. We resort to the anisotropic framework in [19], according to which the source of the anisotropic information is the standard invertible affine map $T_K : \widehat{K} \to K$ between the reference triangle $\widehat{K}$ and the general element K, given by

$$\mathbf{x} = (x_1, x_2)^T = T_K(\widehat{\mathbf{x}}) = M_K \widehat{\mathbf{x}} + \mathbf{t}_K, \quad \forall\, \mathbf{x} \in K,$$

with $\widehat{\mathbf{x}} = (\widehat{x}_1, \widehat{x}_2)^T \in \widehat{K}$. For instance, when $\widehat{K}$ is picked as the equilateral triangle inscribed in the unit circle centered at the origin and with vertices $(-\sqrt{3}/2, -1/2)$, $(\sqrt{3}/2, -1/2)$, $(0, 1)$, it holds

$$M_K = \frac{1}{3} \begin{bmatrix} \sqrt{3}\,(x_1^{K2} - x_1^{K1}) & 2x_1^{K3} - x_1^{K1} - x_1^{K2} \\ \sqrt{3}\,(x_2^{K2} - x_2^{K1}) & 2x_2^{K3} - x_2^{K1} - x_2^{K2} \end{bmatrix},$$

$$\mathbf{t}_K = \frac{1}{3} \begin{bmatrix} x_1^{K1} + x_1^{K2} + x_1^{K3} \\ x_2^{K1} + x_2^{K2} + x_2^{K3} \end{bmatrix},$$

where (x_1^{Ki}, x_2^{Ki}), for $i = 1, 2, 3$, are the vertices of the triangle K.
We introduce the polar decomposition $M_K = B_K\, Z_K$ of M_K, where the matrix B_K is symmetric positive definite and Z_K is orthogonal. Diagonalizing B_K in terms of its eigenvectors $\mathbf{r}_{i,K}$ and eigenvalues $\lambda_{i,K}$, with $i = 1, 2$, yields $B_K = R_K^T \Lambda_K R_K$, where

$$R_K = \begin{bmatrix} \mathbf{r}_{1,K}^T \\ \mathbf{r}_{2,K}^T \end{bmatrix} \quad \text{and} \quad \Lambda_K = \begin{bmatrix} \lambda_{1,K} & 0 \\ 0 & \lambda_{2,K} \end{bmatrix}.$$

The geometrical information provided by the quantities $\lambda_{i,K}, \mathbf{r}_{i,K}$ is displayed in Figure 1. The map T_K strains the circle circumscribed to $\widehat{K}$ into an ellipse circumscribing K, centered at the barycenter of K: the eigenvalues $\lambda_{1,K}, \lambda_{2,K}$ measure the lengths of the major and of the minor semi-axis, aligned with the directions $\mathbf{r}_{1,K}$ and $\mathbf{r}_{2,K}$, respectively. Notice that Z_K and $\mathbf{t}_K$ do not play any role as associated with a rigid rotation and a shift, respectively.
Without loss of generality, henceforth we assume $\lambda_{1,K} \geq \lambda_{2,K}$, i.e., that the so called *stretching factor* $s_K = \lambda_{1,K}/\lambda_{2,K}$, providing us with a measure of the deformation of the triangle K, is always greater than or equal to 1, with $s_K = 1$ whenever K is an equilateral triangle.

3.1 Anisotropic interpolation error estimates

We recall some anisotropic interpolation error estimates proved in [19, 20]. The adjective anisotropic refers to the explicit dependence of these estimates on the geometrical parameters $\lambda_{i,K}, \mathbf{r}_{i,K}$ and s_K, in contrast with the classical isotropic

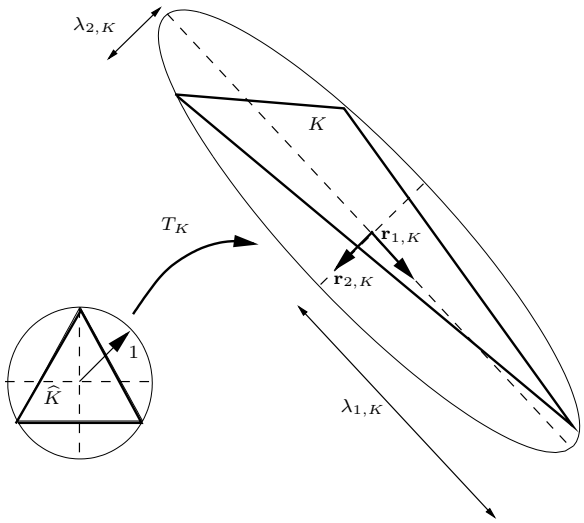

Figure 1: Geometrical interpretation of the map T_K and main anisotropic quantities.

estimates, where the main role is played by the diameter h_K. In particular, we tackle the Clément interpolation operator in [10], defined, in the case of affine finite elements, as

$$I_h^1 v(\mathbf{x}) = \sum_{N_j \in \mathcal{N}_h} P_j v(N_j) \varphi_j(\mathbf{x}) \quad \forall v \in L^2(\Omega), \tag{13}$$

where φ_j is the Lagrangian basis function associated with the node N_j, while P_j denotes the L^2-projection onto the affine functions associated with the patch Δ_j of the elements sharing node N_j, defined by the relations

$$\int_{\Delta_j} (P_j v - v)\psi \; d\Delta_j = 0 \quad \text{with } \psi = 1, x_1, x_2.$$

The sum in (13) runs only on the set $\mathcal{N}_h$ of the internal mesh vertices.

Now for any function $v \in H^1(\Omega)$, let $G_K(v) \in \mathbb{R}^{2\times 2}$ be the symmetric positive semi-definite matrix given by

$$[G_K(v)]_{i,\,j} = \int_{\Delta_K} \frac{\partial v}{\partial x_i} \frac{\partial v}{\partial x_j} \, d\Delta_K, \quad \text{with } i, j = 1, 2, \tag{14}$$

and with Δ_K the union (patch) of all the elements sharing at least a vertex with K.
Then as proved in [19, 20], we have:

Lemma 3.1 *Let $v \in H^1(\Omega)$. Then under the assumptions that, for any K in $\mathcal{T}_h$, $\mathrm{card}(\Delta_K) \le M$ and $\mathrm{diam}(\Delta_{\widehat{K}}) \le \widehat{C}$, with $\Delta_{\widehat{K}} = T_K^{-1}(\Delta_K)$, it holds*

$$\|v - I_h^1 v\|_{L^2(K)} \le C_1 \left[\sum_{i=1}^{2} \lambda_{i,K}^2 \left(\mathbf{r}_{i,K}^T G_K(v) \mathbf{r}_{i,K} \right) \right]^{1/2}, \tag{15}$$

$$\|v - I_h^1 v\|_{L^2(e)} \le C_2 \left(\frac{h_e}{\lambda_{1,K}\lambda_{2,K}} \right)^{1/2} \left[\sum_{i=1}^{2} \lambda_{i,K}^2 \left(\mathbf{r}_{i,K}^T G_K(v) \mathbf{r}_{i,K} \right) \right]^{1/2}, \tag{16}$$

where $C_i = C_i(M, \widehat{C})$, for $i = 1, 2$.

Notice the explicit dependence of these estimates on the anisotropic quantities highlighted in Figure 1. In particular, when $\lambda_{1,K} \simeq \lambda_{2,K} \simeq h_K$, that is when the triangle is equilateral, estimates (15) and (16) reduce to the corresponding isotropic results in [10].
The reference patch $\Delta_{\widehat{K}}$ in Lemma 3.1 is obtained by mapping back all the elements $T \in \Delta_K$ by means of the same transformation T_K^{-1}. The hypotheses in Lemma 3.1 essentially rule out too distorted patches in the reference framework. However the anisotropic features (stretching factor and orientation) of each $T \in \Delta_K$ are not constrained by these requirements; only the variation over Δ_K of the anisotropic quantities is affected (see [27] for more details).

The introduction of the edge stabilization calls for a new anisotropic trace inequality for the directional derivative along a certain direction $\mathbf{d} \in \mathbb{R}^2$. To prove this result we anticipate the estimate

$$\left\| \frac{\partial \widehat{p}}{\partial \widehat{d}} \right\|_{L^2(\widehat{e})} \le \widehat{C}_k \left\| \frac{\partial \widehat{p}}{\partial \widehat{d}} \right\|_{L^2(\widehat{K})} \quad \forall \widehat{p} \in \mathbb{P}_k(\widehat{K}), \tag{17}$$

where $\mathbb{P}_k(\widehat{K})$ is the space of polynomials of maximum global degree k on $\widehat{K}$, $\widehat{e}$ is any edge of $\widehat{K}$, $\widehat{\mathbf{d}}$ is a given unit vector over $\widehat{K}$, and $\widehat{C}_k$ is a constant depending on $\widehat{K}$ and k. Notice that $\widehat{C}_1 = \sqrt{h_{\widehat{e}}/|\widehat{K}|}$. Inequality (17) follows simply by extending the argument used to prove Lemma 2.1 in [34].

Lemma 3.2 *Let $v \in V_h$ and $\mathbf{d}$ be a given unit vector on Ω. Then under the same assumptions as in Lemma 3.1 there exists a constant $C_3 = C_3(|\widehat{K}|)$ such that*

$$\|\nabla v \cdot \mathbf{d}\|_{L^2(e)} \le C_3 \left(\frac{h_e}{\lambda_{1,K}\lambda_{2,K}} \right)^{1/2} \frac{1}{\lambda_{d,K}} \left[\sum_{i=1}^{2} \lambda_{i,K}^2 \left(\mathbf{r}_{i,K}^T G_K(v) \mathbf{r}_{i,K} \right) \right]^{1/2}$$

where

$$\lambda_{d,K} = \left[\lambda_{1,K}^{-2} \big(\mathbf{r}_{1,K} \cdot \mathbf{d} \big)^2 + \lambda_{2,K}^{-2} \big(\mathbf{r}_{2,K} \cdot \mathbf{d} \big)^2 \right]^{-1/2}.$$

Proof. By exploiting the relation $M_K^T \nabla v = \widehat{\nabla} \widehat{v}$ between the gradient on K of v and the gradient on $\widehat{K}$ of $\widehat{v} = v \circ T_K$, and the decompositions introduced on M_K, we have

$$\begin{aligned} \|\nabla v \cdot \mathbf{d}\|^2_{L^2(e)} &= \frac{h_e}{h_{\widehat{e}}} \int_{\widehat{e}} \left[\mathbf{d} \cdot \left(M_K^T\right)^{-1} \widehat{\nabla} \widehat{v}\right]^2 d\widehat{s} = \frac{h_e}{h_{\widehat{e}}} \int_{\widehat{e}} \left[\mathbf{d} \cdot \left(R_K^T \Lambda_K^{-1} R_K Z_K\right) \widehat{\nabla} \widehat{v}\right]^2 d\widehat{s} \\ &= \frac{h_e}{h_{\widehat{e}}} \int_{\widehat{e}} \left[\left(Z_K^T R_K^T \Lambda_K^{-1} R_K \mathbf{d}\right)^T \widehat{\nabla} \widehat{v}\right]^2 d\widehat{s}. \end{aligned}$$

To exploit estimate (17) we let $\mathbf{D} = Z_K^T R_K^T \Lambda_K^{-1} R_K \mathbf{d} = \|\mathbf{D}\|_2 \, \mathbf{1}_{\mathcal{D}}$, where $\mathbf{1}_{\mathcal{D}}$ is a suitable unit vector over $\widehat{K}$, while $\|\mathbf{D}\|_2$ reduces to $\|\Lambda_K^{-1} R_K \mathbf{d}\|_2$, Z_K and R_K being orthogonal matrices. Thus (17) yields

$$\begin{aligned} \|\nabla v \cdot \mathbf{d}\|^2_{L^2(e)} &= \frac{h_e}{h_{\widehat{e}}} \int_{\widehat{e}} \left[\|\mathbf{D}\|_2 \, \mathbf{1}_{\mathcal{D}}^T \widehat{\nabla} \widehat{v}\right]^2 d\widehat{s} = \frac{h_e}{h_{\widehat{e}}} \|\mathbf{D}\|_2^2 \left\| \frac{\partial \widehat{v}}{\partial 1_{\mathcal{D}}} \right\|^2_{L^2(\widehat{e})} \\ &\leq \widehat{C}_1^2 \frac{h_e}{h_{\widehat{e}}} \|\mathbf{D}\|_2^2 \left\| \frac{\partial \widehat{v}}{\partial 1_{\mathcal{D}}} \right\|^2_{L^2(\widehat{K})} \leq \widehat{C}_1^2 \frac{h_e}{h_{\widehat{e}}} \|\mathbf{D}\|_2^2 \, |\widehat{v}|^2_{H^1(\widehat{K})} \\ &\leq \widehat{C}_1^2 \frac{h_e}{h_{\widehat{e}}} \|\mathbf{D}\|_2^2 \left[s_K \left(\mathbf{r}_{1,K}^T \, G_K(v) \, \mathbf{r}_{1,K}\right) + \frac{1}{s_K} \left(\mathbf{r}_{2,K}^T \, G_K(v) \, \mathbf{r}_{2,K}\right) \right], \end{aligned}$$

the last inequality being a direct consequence of relation (17) in [19] and of the definition of s_K. We complete the proof with a straightforward computation of $\|\mathbf{D}\|_2$, yielding $\|\mathbf{D}\|_2 = \lambda_{d,K}^{-1}$, and identifying C_3 with $|\widehat{K}|^{-1/2}$. □

The following result will be useful with a view to the analysis in section 4.

Corollary 3.1 *Under the same hypotheses as in Lemma 3.2 we have that*

$$\|\nabla (I_h w) \cdot \mathbf{d}\|_{L^2(e)} \leq \widetilde{C}_3 \left(\frac{h_e}{\lambda_{1,K} \lambda_{2,K}} \right)^{1/2} \frac{1}{\lambda_{d,K}} \left[\sum_{i=1}^{2} \lambda_{i,K}^2 \, \left(\mathbf{r}_{i,K}^T \, G_K(w) \, \mathbf{r}_{i,K}\right) \right]^{1/2}$$

with $\widetilde{C}_3 = \widetilde{C}_3(M, \widehat{C}, |\widehat{K}|)$.

Proof. We follow the same steps as in the proof of Lemma 3.2 up to the line before the last one, identifying v with $I_h w$ and $\widehat{v}$ with $\widehat{(I_h w)} = \widehat{I}_h \widehat{w}$. This yields

$$\|\nabla (I_h w) \cdot \mathbf{d}\|^2_{L^2(e)} \leq \widehat{C}_1^2 \frac{h_e}{h_{\widehat{e}}} \lambda_{d,K}^{-2} \, |\widehat{I}_h \widehat{w}|^2_{H^1(\widehat{K})}.$$

Now recalling the standard continuity property of the Clément interpolant operator

$$\left|\widehat{I}_h \widehat{w}\right|_{H^1(\widehat{K})} \leq C_I \, |\widehat{w}|_{H^1(\Delta_{\widehat{K}})}$$

with $C_I = C_I(M, \widehat{C})$, combined with (17) in [19], we conclude

$$\|\nabla (I_h w) \cdot \mathbf{d}\|^2_{L^2(e)} \leq \widehat{C}_1^2 \, C_I^2 \frac{h_e}{h_{\widehat{e}}} \lambda_{d,K}^{-2} \left[s_K \left(\mathbf{r}_{1,K}^T \, G_K(w) \, \mathbf{r}_{1,K}\right) + \frac{1}{s_K} \left(\mathbf{r}_{2,K}^T \, G_K(w) \, \mathbf{r}_{2,K}\right) \right],$$

i.e., the desired result with $\widetilde{C}_3 = C_I \, |\widehat{K}|^{-1/2}$. □

4 A posteriori error analysis

To approximating $J(u,q)$ with u and q solution to (4), we derive an a posteriori analysis identifying a discrete pair (u_h, q_h) such that $|J(u,q)-J(u_h,q_h)|$ is within to a desired tolerance. The idea is to exploit the a posteriori estimator to build the most economical grid for approximating both u and q, in addition "sensitive" to the functional of interest J, in the spirit of a goal oriented approach (see, e.g., [4, 22, 26, 30]).
In more detail, the actual purpose is to enrich the a posteriori analysis in [3] with the anisotropic information of section 3. The anisotropic mesh adaptation help us in getting the most effective mesh from the computational viewpoint.

Before stating the main result of the paper we anticipate some notation. Hereafter we assume $n(q,r) = \alpha(q,r)$, i.e., coinciding with the standard L^2-scalar product weighted by a positive constant α.
Let

$$\rho_K^u = \big(f + q + \nabla\cdot(\varepsilon\nabla u_h) - \boldsymbol{\beta}\cdot\nabla u_h - \sigma u_h\big)\big|_K \tag{18}$$

and

$$R_{K_e}^u = \begin{cases} \big[\varepsilon\nabla u_h\cdot\mathbf{n}\big]_e & \text{if } e\in\mathcal{E}_h\backslash\partial\Omega \\ 0 & \text{if } e\in\partial\Omega \end{cases} \tag{19}$$

be the element internal and boundary state residual, respectively; let

$$\rho_K^\lambda = \big(c(c_0 - cu_h) + \nabla\cdot(\varepsilon\nabla\lambda_h) + \boldsymbol{\beta}\cdot\nabla\lambda_h - \sigma\lambda_h\big)\big|_K \tag{20}$$

and

$$R_{K_e}^\lambda = \begin{cases} \big[\varepsilon\nabla\lambda_h\cdot\mathbf{n}\big]_e & \text{if } e\in\mathcal{E}_h\backslash\partial\Omega \\ 0 & \text{if } e\in\partial\Omega \end{cases} \tag{21}$$

be the element internal and boundary adjoint state residual, respectively; finally let

$$\rho_K^q = \big(\alpha q_h - \lambda_h\big)\big|_K \tag{22}$$

be the gradient residual.

Proposition 4.1 *Let $\{u,\lambda,q\}\in V\times V\times Q$ be the solution to (5) and $\{u_h,\lambda_h,q_h\}\in V_h\times V_h\times Q_h$ be the corresponding approximation, solution to (6)-(8). Moreover let $q\in H^1(\Omega)$, and the observation operator $c(\cdot)$ in (3) be identified by a function in $L^\infty(\Omega)$. Then, under the hypotheses as in Lemma 3.1,*

$$\big|J(u,q) - J(u_h,q_h)\big| \le C\sum_{K\in\mathcal{T}_h}\Big\{\mathcal{R}_K^u\omega_K(\lambda) + \mathcal{R}_K^\lambda\omega_K(u) + \mathcal{R}_K^q\omega_K(q)\Big\}, \tag{23}$$

where $J(u,q)$ is the cost functional in (3), $C = C(M, \widehat{C}, |\widehat{K}|)$, the residuals $\mathcal{R}_K^u$, $\mathcal{R}_K^\lambda$ and $\mathcal{R}_K^q$ are identified by

$$\mathcal{R}_K^u = \left(\frac{1}{\lambda_{1,K}\lambda_{2,K}}\right)^{1/2} \sum_{e\in\partial K} \left(\frac{h_e^{1/2}}{2} \|R_{K_e}^u\|_{L^2(e)} + \frac{h_e^{3/2}}{\lambda_{n_e,K}} \|\gamma\|_{L^\infty(e)} \|[\nabla u_h \cdot \mathbf{n}]_e\|_{L^2(e)} \right) + \|\rho_K^u\|_{L^2(K)},$$

$$\mathcal{R}_K^\lambda = \left(\frac{1}{\lambda_{1,K}\lambda_{2,K}}\right)^{1/2} \sum_{e\in\partial K} \left(\frac{h_e^{1/2}}{2} \|R_{K_e}^\lambda\|_{L^2(e)} + \frac{h_e^{3/2}}{\lambda_{n_e,K}} \|\gamma\|_{L^\infty(e)} \|[\nabla \lambda_h \cdot \mathbf{n}]_e\|_{L^2(e)} \right) + \|\rho_K^\lambda\|_{L^2(K)},$$

$$\mathcal{R}_K^q = \|\rho_K^q\|_{L^2(K)},$$

the weights $\omega_K(u)$, $\omega_K(\lambda)$ and $\omega_K(q)$ are given by

$$\begin{aligned} \omega_K(u) &= \left[\sum_{i=1}^{2} \lambda_{i,K}^2 \left(\mathbf{r}_{i,K}^T G_K(u) \mathbf{r}_{i,K} \right) \right]^{1/2}, \\ \omega_K(\lambda) &= \left[\sum_{i=1}^{2} \lambda_{i,K}^2 \left(\mathbf{r}_{i,K}^T G_K(\lambda) \mathbf{r}_{i,K} \right) \right]^{1/2}, \\ \omega_K(q) &= \left[\sum_{i=1}^{2} \lambda_{i,K}^2 \left(\mathbf{r}_{i,K}^T G_K(q) \mathbf{r}_{i,K} \right) \right]^{1/2}, \end{aligned} \tag{24}$$

all the element internal and boundary residuals being defined as in (18)-(22).

Proof. By mimicking the proof of Proposition 4.1 in [3] we get the initial relation

$$J(u,q) - J(u_h,q_h) = \frac{1}{2} \nabla \mathcal{L}_{stab}(u_h,\lambda_h,q_h)(u - I_h u, \lambda - I_h\lambda, q - I_h q). \tag{25}$$

Plugging the expression of the gradient of $\mathcal{L}_{stab}$ in (11) in this identity, we obtain

$$\begin{aligned} J(u,q) - J(u_h,q_h) &= \frac{1}{2} \nabla \mathcal{L}_{stab}(u_h,\lambda_h,q_h)(u - I_h u, \lambda - I_h\lambda, q - I_h q) \\ &= \frac{1}{2}\Big[a(u_h, \lambda - I_h\lambda) - b(q_h, \lambda - I_h\lambda) - (f, \lambda - I_h\lambda) \\ &+ \frac{1}{2} \sum_{K\in\mathcal{T}_h} \Big\{ \sum_{e\in\partial K} \int_e \gamma\, h_e^2 \, [\nabla u_h \cdot \mathbf{n}]_e \, [\nabla(\lambda - I_h\lambda)\cdot \mathbf{n}]_e \, ds \Big\} \Big] \\ &+ \frac{1}{2}\Big[a(u - I_h u, \lambda_h) + (cu_h - c_0, c(u - I_h u)) \\ &+ \frac{1}{2} \sum_{K\in\mathcal{T}_h} \Big\{ \sum_{e\in\partial K} \int_e \gamma\, h_e^2 \, [\nabla(u - I_h u) \cdot \mathbf{n}]_e \, [\nabla \lambda_h \cdot \mathbf{n}]_e \, ds \Big\} \Big] \\ &- \frac{1}{2}\Big[b(q - I_h q, \lambda_h) - n(q_h, q - I_h q) \Big] \\ &= \frac{1}{2}\big[\mathcal{I}_u + \mathcal{I}_{u,stab}\big] + \frac{1}{2}\big[\mathcal{I}_\lambda + \mathcal{I}_{\lambda,stab}\big] + \frac{1}{2}\big[\mathcal{I}_q\big]. \end{aligned} \tag{26}$$

Let us deal with the five terms on the right-hand side of (26) in turn.
We point out that C will denote different constant values throughout the proof.
The definitions of the bilinear forms $a(\cdot,\cdot)$ and $b(\cdot,\cdot)$, elementwise integration by parts of the diffusive term, and the definitions (18) and (19) of the internal and boundary state residuals yield

$$\begin{aligned}
\mathcal{I}_u &= a(u_h, \lambda - I_h\lambda) - b(q_h, \lambda - I_h\lambda) - (f, \lambda - I_h\lambda) \\
&= \sum_{K\in\mathcal{T}_h} \Big\{ \int_K \varepsilon \nabla u_h \cdot \nabla(\lambda - I_h\lambda)\, dK + \int_K \boldsymbol{\beta}\cdot\nabla u_h (\lambda - I_h\lambda)\, dK \\
&+ \int_K \sigma u_h (\lambda - I_h\lambda)\, dK - \int_K q_h(\lambda - I_h\lambda)\, dK - \int_K f(\lambda - I_h\lambda)\, dK \Big\} \\
&= \sum_{K\in\mathcal{T}_h} \Big\{ \int_K \Big[\nabla\cdot(\varepsilon\nabla u_h) + \boldsymbol{\beta}\cdot\nabla u_h + \sigma u_h - f - q\Big](\lambda - I_h\lambda)\, dK \\
&+ \frac{1}{2}\sum_{e\in\partial K} \int_e \Big[\varepsilon \frac{\partial u_h}{\partial n}\Big]_e (\lambda - I_h\lambda)\, ds \Big\} \\
&= \sum_{K\in\mathcal{T}_h} \Big\{ \int_K -\rho_K^u(\lambda - I_h\lambda)\, dK + \frac{1}{2}\sum_{e\in\partial K}\int_e R^u_{K_e}(\lambda - I_h\lambda)\, ds \Big\}.
\end{aligned} \tag{27}$$

Via the Cauchy-Schwarz inequality and Lemma 3.1, we have

$$\begin{aligned}
|\mathcal{I}_u| \le\ & C \sum_{K\in\mathcal{T}_h} \Big\{ \Big[\|\rho_K^u\|_{L^2(K)} + \frac{1}{2}\Big(\frac{1}{\lambda_{1,K}\lambda_{2,K}}\Big)^{1/2} \Big(\sum_{e\in\partial K} \|R^u_{K_e}\|_{L^2(e)}\, h_e^{1/2}\Big)\Big] \\
& \Big[\sum_{i=1}^{2} \lambda_{i,K}^2 \ \big(\mathbf{r}_{i,K}^T\, G_K(\lambda)\, \mathbf{r}_{i,K}\big)\Big]^{1/2} \Big\},
\end{aligned} \tag{28}$$

with $C = \max(C_1, C_2)$. Let us consider now $\mathcal{I}_{u,stab}$. Exploiting the regularity of λ and suitably redistributing elementwise the jump $[-\nabla(I_h\lambda)\cdot\mathbf{n}]_e$, provide us with

$$\begin{aligned}
\mathcal{I}_{u,stab} &= \frac{1}{2}\sum_{K\in\mathcal{T}_h} \Big\{ \sum_{e\in\partial K} \int_e \gamma\, h_e^2\, [\nabla u_h\cdot\mathbf{n}]_e\, [\nabla(\lambda - I_h\lambda)\cdot\mathbf{n}]_e\, ds \Big\} \\
&= \sum_{K\in\mathcal{T}_h} \Big\{ \sum_{e\in\partial K} \int_e \gamma\, h_e^2\, [\nabla u_h\cdot\mathbf{n}]_e \big(-\nabla(I_h\lambda)\cdot\mathbf{n}_{e,K}\big)\, ds \Big\}
\end{aligned}$$

where $\mathbf{n}_{e,K} = \mathbf{n}_K\big|_e$, for $e\in\partial K$. Cauchy-Schwarz inequality and Corollary 3.1 lead to

$$\begin{aligned}
|\mathcal{I}_{u,stab}| &\le \sum_{K\in\mathcal{T}_h} \Big\{ \sum_{e\in\partial K} \|\gamma\|_{L^\infty(e)}\, h_e^2\, \|[\nabla u_h\cdot\mathbf{n}]_e\|_{L^2(e)}\, \|\nabla(I_h\lambda)\cdot\mathbf{n}_{e,K}\|_{L^2(e)} \Big\} \\
&\le \widetilde{C}_3 \sum_{K\in\mathcal{T}_h} \Big\{ \Big(\sum_{e\in\partial K} \|\gamma\|_{L^\infty(e)}\, \frac{h_e^{3/2}}{\lambda_{n_e,K}}\, \|[\nabla u_h\cdot\mathbf{n}]_e\|_{L^2(e)}\Big) \\
&\quad \Big(\frac{1}{\lambda_{1,K}\lambda_{2,K}}\Big)^{1/2} \Big[\sum_{i=1}^{2} \lambda_{i,K}^2 \ \big(\mathbf{r}_{i,K}^T\, G_K(\lambda)\, \mathbf{r}_{i,K}\big)\Big]^{1/2} \Big\}.
\end{aligned} \tag{29}$$

In the same fashion as the one driving to (27), we obtain

$$\mathcal{I}_\lambda = \sum_{K\in\mathcal{T}_h} \Big\{ \int_K -\rho_K^\lambda (u - I_h u)\, dK + \frac{1}{2} \sum_{e\in\partial K} \int_e R_{K_e}^\lambda (u - I_h u)\, ds \Big\}.$$

Cauchy-Schwarz inequality and the anisotropic estimates (15) and (16) give

$$\begin{aligned} |\mathcal{I}_\lambda| \;\leq\; & C \sum_{K\in\mathcal{T}_h} \Big\{ \Big[\|\rho_K^\lambda\|_{L^2(K)} + \frac{1}{2} \Big(\frac{1}{\lambda_{1,K}\lambda_{2,K}} \Big)^{1/2} \Big(\sum_{e\in\partial K} \|R_{K_e}^\lambda\|_{L^2(e)}\, h_e^{1/2} \Big) \Big] \\ & \Big[\sum_{i=1}^{2} \lambda_{i,K}^2 \, \big(\mathbf{r}_{i,K}^T\, G_K(u)\, \mathbf{r}_{i,K} \big) \Big]^{1/2} \Big\}, \end{aligned} \tag{30}$$

with $C = \max(C_1, C_2)$. The term $\mathcal{I}_{\lambda,stab}$ can be bounded exactly as $\mathcal{I}_{u,stab}$, i.e.,

$$\begin{aligned} |\mathcal{I}_{\lambda,stab}| \;\leq\; & \widetilde{C}_3 \sum_{K\in\mathcal{T}_h} \Big\{ \Big(\sum_{e\in\partial K} \|\gamma\|_{L^\infty(e)} \frac{h_e^{3/2}}{\lambda_{n_e,K}} \|[\nabla\lambda_h \cdot \mathbf{n}]_e\|_{L^2(e)} \Big) \\ & \Big(\frac{1}{\lambda_{1,K}\lambda_{2,K}} \Big)^{1/2} \Big[\sum_{i=1}^{2} \lambda_{i,K}^2 \, \big(\mathbf{r}_{i,K}^T\, G_K(u)\, \mathbf{r}_{i,K} \big) \Big]^{1/2} \Big\}. \end{aligned} \tag{31}$$

Eventually, the gradient contribution I_q is managed recalling the definition of the bilinear form $b(\cdot,\cdot)$, the choice made for the Tikhonov regularization $n(q,q)$ in (3), and using the Cauchy-Schwarz inequality and estimate (15) as

$$\begin{aligned} |\mathcal{I}_q| \;\leq\; & \sum_{K\in\mathcal{T}_h} \|\rho_K^q\|_{L^2(K)}\, \|q - I_h q\|_{L^2(K)} \\ \leq\; & C \sum_{K\in\mathcal{T}_h} \Big\{ \|\rho_K^q\|_{L^2(K)} \Big[\sum_{i=1}^{2} \lambda_{i,K}^2 \, \big(\mathbf{r}_{i,K}^T\, G_K(q)\, \mathbf{r}_{i,K} \big) \Big]^{1/2} \Big\}, \end{aligned} \tag{32}$$

with $C = C_1$. The final result (23) follows after suitably gathering (28), (29), (30), (31) and (32). □

Estimate (23) enjoys the same structure as in [3]: the residual of the state equation is weighted by $\omega_K(\lambda)$ which is related to the adjoint state variable; vice versa the adjoint state residual is tuned by the weight associated with the state variable u; the gradient residual is modulated by the control variable itself via $\omega_K(q)$.
The added value of estimate (23) with respect to [3] is the presence of anisotropic information, lumped in the weights.

Remark 4.1 *An a posteriori estimate alternative to (23) and enjoying the same structure can be obtained in the same spirit as in [13]. In more detail, a different choice for the discrete test function φ_h in (4.5) of [4], leads to replacing in (25), e.g., $u - I_h u$ with $u - u_h - I_h(u - u_h)$, and analogously for the adjoint state and the control variables. We get consequently weights depending on the interpolation errors in the right-hand side of (23). As numerically assessed in [13] this last approach yields more economical grids in the case of the Clément interpolant.*

The right-hand side of (23) still involves the exact optimal solution $\{u, \lambda, q\}$, thus not being directly computable. To make such a quantity operative with a view to the mesh adaptive algorithm, we introduce a suitable recovery procedure. Namely, as the weights depend on the first order partial derivatives of $\{u, \lambda, q\}$ via the matrix G_K in (14), we resort to the standard area-weighted Zienkiewicz-Zhu gradient recovery procedure ([36, 37, 33, 28]). Hence the general matrix $G_K(z)$, for any $z \in H^1(\Omega)$, is replaced by $G_K^*(z)$, where

$$[G_K^*(z)]_{i,\,j} = \int_{\Delta_K} (\nabla^{ZZ} z)_i \, (\nabla^{ZZ} z)_j \, d\Delta_K, \quad \text{with } i, j = 1, 2,$$

$\nabla^{ZZ} z = ((\nabla^{ZZ} z)_1, (\nabla^{ZZ} z)_2)^T$ denoting the recovered gradient obtained from the discrete approximation z_h.

The global error estimator for the cost functional $J(u, q)$ in (3) stemming from Proposition 4.1 is thus identified by

$$\eta_J = \sum_{K \in \mathcal{T}_h} \eta_K, \tag{33}$$

where $\eta_K = \mathcal{R}_K^u \omega_K^*(\lambda) + \mathcal{R}_K^\lambda \omega_K^*(u) + \mathcal{R}_K^q \omega_K^*(q)$ is the corresponding local error estimator, with

$$\begin{aligned}
\omega_K^*(u) &= \left[\sum_{i=1}^{2} \lambda_{i,K}^2 \, \left(\mathbf{r}_{i,K}^T \, G_K^*(u) \, \mathbf{r}_{i,K} \right) \right]^{1/2}, \\
\omega_K^*(\lambda) &= \left[\sum_{i=1}^{2} \lambda_{i,K}^2 \, \left(\mathbf{r}_{i,K}^T \, G_K^*(\lambda) \, \mathbf{r}_{i,K} \right) \right]^{1/2}, \\
\omega_K^*(q) &= \left[\sum_{i=1}^{2} \lambda_{i,K}^2 \, \left(\mathbf{r}_{i,K}^T \, G_K^*(q) \, \mathbf{r}_{i,K} \right) \right]^{1/2}.
\end{aligned}$$

We point out that constant C in (23) is dropped in the definition of η_J. However it may be taken into account by a suitable tuning, as depending only on quantities related to $\widehat{K}$ and $\Delta_{\widehat{K}}$. Finally we highlight that when $\lambda_{1,K} \simeq \lambda_{2,K} \simeq h_K$ we recover the corresponding isotropic a posteriori error estimator.

5 The adaptive procedure

This section is devoted to presenting the iterative procedure followed to commute the a posteriori error estimator in (33) into an actual algorithm to anisotropically adapt the computational mesh. Concerning the optimization procedure, we provide the details separately for the two test cases, as a different algorithm is employed for each of them.

5.1 The mesh adaptation procedure

We employ a *metric-based* adaptive procedure as a predictive tool. Two reciprocal approaches are pursuable: either given a constraint on the maximum number of elements, find the mesh providing the most accurate numerical solution; or given a constraint on the accuracy of the numerical solution, find the mesh with the least number of elements. We here focus on the latter approach.

We recall that a metric is induced by a symmetric positive-definite tensor field $\widetilde{M} : \Omega \to \mathbb{R}^{2\times 2}$ (see, e.g., [21]). Let us emphasize the link existing between metric and mesh. With any given mesh $\mathcal{T}_h$, we associate a piecewise constant metric $\widetilde{M}_{\mathcal{T}_h}$, such that $\widetilde{M}_{\mathcal{T}_h}|_K = \widetilde{M}_K = B_K^{-2} = R_K^T \Lambda_K^{-2} R_K$, for any $K \in \mathcal{T}_h$, the matrices R_K and Λ_K being defined according to section 3. With respect to this metric, any triangle K is unit equilateral, i.e. $\sqrt{\mathbf{e}^T \widetilde{M}_{\mathcal{T}_h} \mathbf{e}} = 1$, with $\mathbf{e}$ the vector identifying the edge e of K.

Vice versa let now $\widetilde{M}$ be a given metric. We show how an optimal mesh $\mathcal{T}_h$ with respect to $\widetilde{M}$ can be defined in terms of a so-called *matching condition*. We first diagonalize the tensor field $\widetilde{M}$ as $\widetilde{M} = \widetilde{R}^T \widetilde{\Lambda}^{-2} \widetilde{R}$, with $\widetilde{\Lambda} = \mathrm{diag}(\widetilde{\lambda}_1, \widetilde{\lambda}_2)$ and $\widetilde{R}^T = [\widetilde{\mathbf{r}}_1, \widetilde{\mathbf{r}}_2]$ a positive diagonal and an orthogonal matrix, respectively. We then approximate the quantities $\widetilde{\lambda}_1$, $\widetilde{\lambda}_2$, $\widetilde{\mathbf{r}}_1$ and $\widetilde{\mathbf{r}}_2$ via piecewise constants over $\mathcal{T}_h$, such that $\widetilde{\mathbf{r}}_i|_K = \widetilde{\mathbf{r}}_{i,K} \in \mathbb{R}^2$, $\widetilde{\lambda}_i|_K = \widetilde{\lambda}_{i,K} \in \mathbb{R}$, for any $K \in \mathcal{T}_h$ and with $i = 1, 2$.

Thus following Definition 5.1 in [29] we state that the mesh $\mathcal{T}_h$ matches $\widetilde{M}$ if, for any $K \in \mathcal{T}_h$, $\widetilde{M}|_K = \widetilde{M}_{\mathcal{T}_h}|_K$, i.e., $\widetilde{\mathbf{r}}_{i,K} = \mathbf{r}_{i,K}$, $\widetilde{\lambda}_{i,K} = \lambda_{i,K}$, for $i = 1, 2$.
In the spirit of a predictive procedure the tensor field $\widetilde{M}$ represents the actual unknown. In more detail, the computation of $\widetilde{M}$ (and of the corresponding matching triangulation) is obtained via an iterative procedure. At each iteration, say j, we deal with three quantities:

i) the actual mesh $\mathcal{T}_h^{(j)}$;

ii) the new metric $\widetilde{M}^{(j+1)}$ computed on $\mathcal{T}_h^{(j)}$;

iii) the updated mesh $\mathcal{T}_h^{(j+1)}$ matching $\widetilde{M}^{(j+1)}$.

Problem (6)-(8) is solved on $\mathcal{T}_h^{(j)}$ and the corresponding solution $\{u_h, \lambda_h, q_h\}$ drives suitable local minimization problems (one for each $K \in \mathcal{T}_h^{(j)}$), with the aim of identifying the metric $\widetilde{M}^{(j+1)}$. Finally the new mesh $\mathcal{T}_h^{(j+1)}$ is built via the matching condition. This last task is accomplished by means of the function `adaptmesh` in `FreeFem++` ([23]).

Before addressing the local minimization problem, we suitably rewrite the local estimator η_K in (33) as

$$\eta_K = \overline{\alpha}_K \left\{ \overline{\mathcal{R}}_K^u \, \overline{\omega}_K^*(\lambda) + \overline{\mathcal{R}}_K^\lambda \, \overline{\omega}_K^*(u) + \overline{\mathcal{R}}_K^q \, \overline{\omega}_K^*(q) \right\} \tag{34}$$

where $\overline{\alpha}_K = \lambda_{1,K}^{3/2}\lambda_{2,K}^{3/2}$ gathers all the area $|K|$ information,

$$\overline{\mathcal{R}}_K^u = \frac{\mathcal{R}_K^u}{\lambda_{1,K}^{1/2}\lambda_{2,K}^{1/2}}, \quad \overline{\mathcal{R}}_K^\lambda = \frac{\mathcal{R}_K^\lambda}{\lambda_{1,K}^{1/2}\lambda_{2,K}^{1/2}}, \quad \overline{\mathcal{R}}_K^q = \frac{\mathcal{R}_K^q}{\lambda_{1,K}^{1/2}\lambda_{2,K}^{1/2}},$$

are approximately pointwise values (at least for a sufficiently fine mesh), while the new weights

$$\begin{aligned}
\overline{\omega}_K^*(u) &= \left[s_K\,\mathbf{r}_{1,K}^T\,\overline{G}_K^*(u)\,\mathbf{r}_{1,K} + \frac{1}{s_K}\,\mathbf{r}_{2,K}^T\,\overline{G}_K^*(u)\,\mathbf{r}_{2,K}\right]^{1/2},\\
\overline{\omega}_K^*(\lambda) &= \left[s_K\,\mathbf{r}_{1,K}^T\,\overline{G}_K^*(\lambda)\,\mathbf{r}_{1,K} + \frac{1}{s_K}\,\mathbf{r}_{2,K}^T\,\overline{G}_K^*(\lambda)\,\mathbf{r}_{2,K}\right]^{1/2},\\
\overline{\omega}_K^*(q) &= \left[s_K\,\mathbf{r}_{1,K}^T\,\overline{G}_K^*(q)\,\mathbf{r}_{1,K} + \frac{1}{s_K}\,\mathbf{r}_{2,K}^T\,\overline{G}_K^*(q)\,\mathbf{r}_{2,K}\right]^{1/2}
\end{aligned}$$

collect only the anisotropic information associated with K, with $\overline{G}_K^*(\cdot) = G_K^*(\cdot)$ $(\lambda_{1,K}\lambda_{2,K})^{-1}$. Following [29], for ease of computation we suitably combine the information of the three terms in (34) in a single one. This yields

$$\eta_K = \overline{\alpha}_K\,\overline{\omega}_K^*$$

with $\overline{\alpha}_K$ defined as in (34) and

$$\overline{\omega}_K^* = \left[s_K\,\mathbf{r}_{1,K}^T\,\overline{G}_K^*\,\mathbf{r}_{1,K} + \frac{1}{s_K}\,\mathbf{r}_{2,K}^T\,\overline{G}_K^*\,\mathbf{r}_{2,K}\right]^{1/2},$$

where the local matrix

$$\overline{G}_K^* = \left(\overline{\mathcal{R}}_K^u\right)^2\overline{G}_K^*(\lambda) + \left(\overline{\mathcal{R}}_K^\lambda\right)^2\overline{G}_K^*(u) + \left(\overline{\mathcal{R}}_K^q\right)^2\overline{G}_K^*(q) \tag{35}$$

merges the anisotropic information provided by the state, the adjoint state and the control variable, respectively, suitably weighted via the local residuals. The adaptive procedure based on $\overline{G}_K^*$ will be able to take into account all the directional features associated simultaneously with the three independent variables u, λ and q (we refer to section 6 for some details).

We are now in a position to discuss the local problem aiming at minimizing the number of mesh elements. We first observe that this is equivalent to maximizing the area of each element. In the spirit of an equidistribution criterion, we enforce also that, for each element $K \in \mathcal{T}_h^{(j+1)}$, $\eta_K = \overline{\alpha}_K\,\overline{\omega}_K^* = \tau$, with τ a local tolerance. Thus the goal of maximizing the area $|K| = |\widehat{K}|\,\lambda_{1,K}\lambda_{2,K}$ lumped into $\overline{\alpha}_K$ is achieved by minimizing the weight $\overline{\omega}_K^*$ with respect to s_K and $\mathbf{r}_{1,K}$, i.e., by solving the local constrained minimization

$$\min_{s_K \geq 1, \mathbf{r}_{i,K}\cdot\mathbf{r}_{j,K} = \delta_{ij}} \overline{\omega}_K^*(\mathbf{r}_{1,K}, s_K), \tag{36}$$

δ_{ij} being the Kronecker symbol and where it is understood that $\mathbf{r}_{1,K}$ and $\mathbf{r}_{2,K}$ are orthonormal vectors. Notice that all the recovered quantities involved in $\overline{\omega}_K^*$ are computed on the background grid $\mathcal{T}_h^{(j)}$.

The following statement provides us with the desired result:

Proposition 5.1 *Let $\{\mathbf{l}_{i,K}, g_{i,K}\}$ be the eigenvector-eigenvalue pair of $\overline{G}_K^*$ with $g_{1,K} \geq g_{2,K} > 0$. Then the minimum (36) is identified by the choices*

$$\widetilde{\mathbf{r}}_{1,K} = \mathbf{l}_{2,K} \quad \textit{and} \quad \widetilde{s}_K = \left(\frac{g_{1,K}}{g_{2,K}}\right)^{1/2}, \tag{37}$$

yielding the value $\left(2\sqrt{g_{1,K}g_{2,K}}\right)^{1/2}$ for $\overline{\omega}_K^*$.

Proof. We refer to Proposition 14 in [18]. □

We observe that the optimal weight $\overline{\omega}_K^*$ does not depend on the stretching factor. This sounds promising with a view to the efficiency and reliability analysis of the error estimator η_J.

To complete the construction of the optimal metric $\widetilde{M}^{(j+1)}$, it suffices to extract the separate values of $\widetilde{\lambda}_{1,K}$ and $\widetilde{\lambda}_{2,K}$ obtained by directly exploiting the equidistribution constraint, i.e., solving the equations

$$\left(\widetilde{\lambda}_{1,K}\widetilde{\lambda}_{2,K}\right)^{3/2}\left(2\sqrt{g_{1,K}g_{2,K}}\right)^{1/2} = \tau \quad \text{and} \quad \frac{\widetilde{\lambda}_{1,K}}{\widetilde{\lambda}_{2,K}} = \widetilde{s}_K = \left(\frac{g_{1,K}}{g_{2,K}}\right)^{1/2}. \tag{38}$$

System (38) provides us with the distinct values

$$\widetilde{\lambda}_{1,K} = \left(\frac{1}{\sqrt{2}}\left(\frac{g_{1,K}}{g_{2,K}^2}\right)^{1/2}\tau\right)^{1/3}, \quad \widetilde{\lambda}_{2,K} = \left(\frac{1}{\sqrt{2}}\left(\frac{g_{2,K}}{g_{1,K}^2}\right)^{1/2}\tau\right)^{1/3}. \tag{39}$$

Eventually, the optimal metric $\widetilde{M}^{(j+1)}$ is identified by $\widetilde{\mathbf{r}}_{1,K}$ in (37), $\widetilde{\lambda}_{1,K}$ and $\widetilde{\lambda}_{2,K}$ in (39), with $\widetilde{\mathbf{r}}_{2,K} \perp \widetilde{\mathbf{r}}_{1,K}$.

To summarize, the adaptive algorithm used in practice is:

Algorithm 5.1 `Set` $j = 0$`:`

1. `build the background mesh` $\mathcal{T}_h^{(j)}$`;`
2. `solve problem (6)-(8);`
3. `solve the local minimization problem (36) for the pair` $(\widetilde{s}_K, \widetilde{\mathbf{r}}_{1,K})$`;`
4. `via the equidistribution principle, compute` $(\widetilde{\lambda}_{1,K}, \widetilde{\lambda}_{2,K})$ `by (38)-(39);`
5. `build up the new metric` $\widetilde{M}^{(j+1)}$`;`

6. construct the new mesh $\mathcal{T}_h^{(j+1)}$ matching $\widetilde{M}^{(j+1)}$;

7. if a suitable stopping criterion is met, exit; else $j \leftarrow j+1$ and go to 2.

As possible stopping criterion, we can fix the maximum number of iterations rather than $|\#\mathcal{T}_h^{(j+1)} - \#\mathcal{T}_h^{(j)}| \leq \#\mathcal{T}_h^{(j)}\,\mathtt{TOLL_{REL}}$, for a small relative tolerance $\mathtt{TOLL_{REL}}$.

Remark 5.1 *When the metric-based approach is driven by the maximization of the solution accuracy for a fixed number of elements,* `Algorithm 5.1` *can still be used provided that the local tolerance τ in (38) is suitably modified.*

6 Numerical results

We consider two test cases: the first is an academic benchmark, whereas the second deals with a problem of possible interest in an environmental framework. In both cases our purpose is to assess qualitatively the performance of the adaptive procedure in section 5. A deeper analysis from a quantitative viewpoint is forthcoming.
We point out that the numerical tests below employ the modified estimator proposed in Remark 4.1. Moreover the tuning parameter γ_0 in (9) of the edge stabilization term is set equal to 10^{-2}.

6.1 A benchmark problem

We start from a relatively simple framework fitting thoroughly (4), but at the same time exhibiting directional features. Namely, we refer to Example 1 in section 5.1 in [1]. The domain Ω coincides with the rectangle $(0,1)\times(0,0.2)$; the diffusion coefficient is $\varepsilon = 10^{-3}$; the advective field is $\boldsymbol{\beta} = 2\pi\left(x_2-0.1, x_1-0.5\right)^T$ (see Figure 2 (left)); the reaction σ is equal to 1; the source term is $f = 0$.
With reference to (3), we pick $c = 1$, c_0 (see Figure 2 (right)) as the solution to (1) with the above data except that

$$f = 5\Big\{\exp\Big(-\frac{(x_1-0.2)^2+(x_2-0.1)^2}{0.02}\Big) + \exp\Big(-\frac{(x_1-0.8)^2+(x_2-0.1)^2}{0.02}\Big)\Big\},$$

while $n(q,q) = \alpha\int_\Omega q^2\,d\Omega$. Two different choices are made for the Tikhonov regularization parameter α. The expected solution u to (4) should be a "perturbation" of c_0, as small as possible, the smaller α. The observation function c_0 reaches its maximum values along the 45° diagonal passing through the center of the domain. It is also characterized by steep boundary layers all along the outflow of the domain.

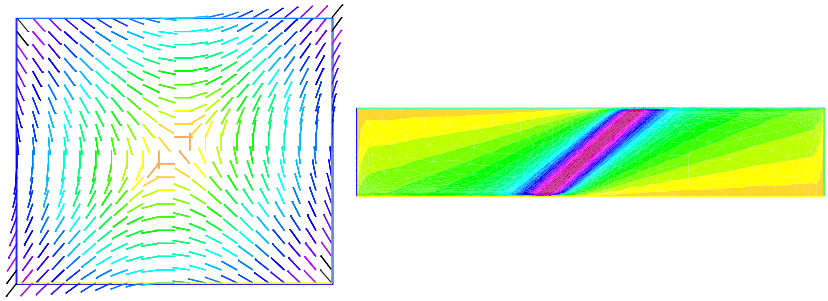

Figure 2: Advective field $\boldsymbol{\beta}$ and observation c_0 for the benchmark problem.

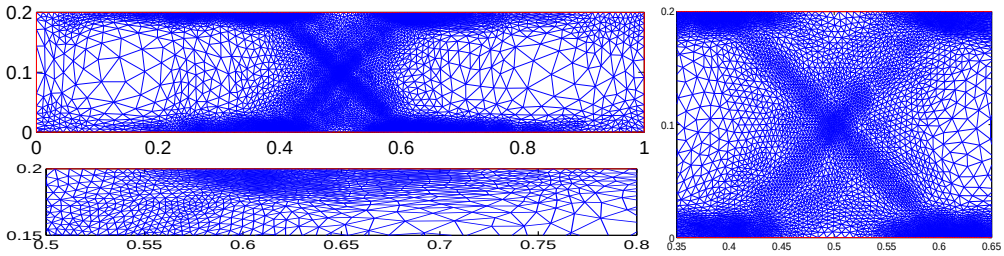

Figure 3: Second adapted grid for the benchmark problem and for $\alpha = 1$: global grid (top-left); a zoom around the center of Ω (right); a detail of the upper-right boundary layer (bottom-left).

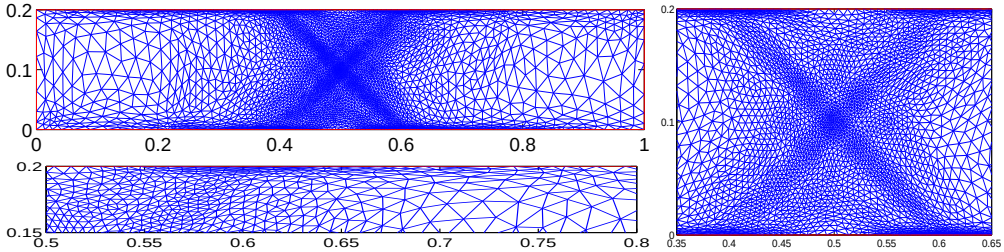

Figure 4: Final adapted grid for the benchmark problem and for $\alpha = 1$: global grid (top-left); a zoom around the center of Ω (right); a detail of the upper-right boundary layer (bottom-left).

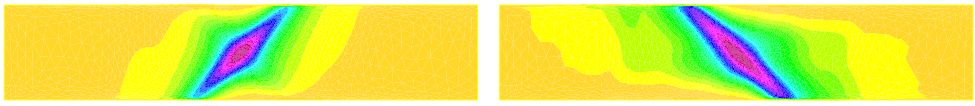

Figure 5: State (left) and adjoint state (right) solutions to the benchmark problem on the last adapted grid for $\alpha = 1$.

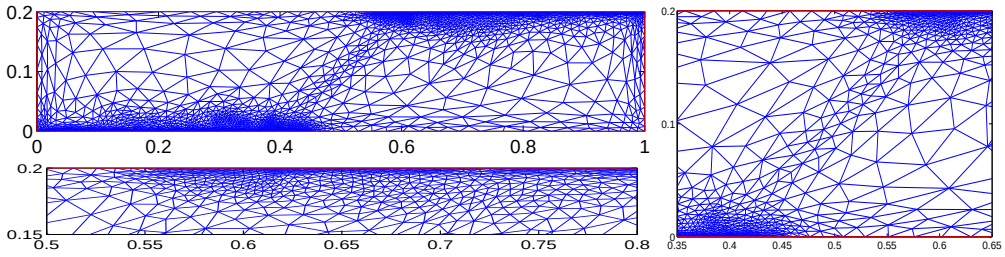

Figure 6: Third adapted grid for the benchmark problem and for $\alpha = 10^{-4}$: global grid (top-left); a zoom around the center of Ω (right); a detail of the upper-right boundary layer (bottom-left).

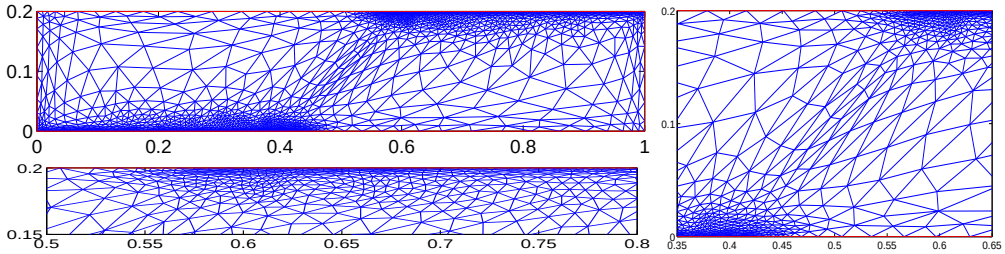

Figure 7: Final adapted grid for the benchmark problem and for $\alpha = 10^{-4}$: global grid (top-left); a zoom around the center of Ω (right); a detail of the upper-right boundary layer (bottom-left).

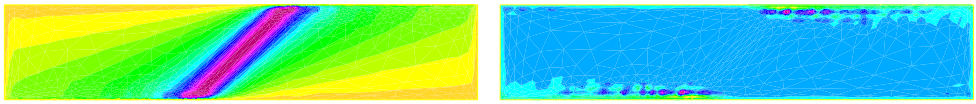

Figure 8: State (left) and adjoint state (right) solutions to the benchmark problem on the last adapted grid for $\alpha = 10^{-4}$.

The linear system arising from the discrete equations (6)-(8) is solved by the sparse LU-decomposition in UMFPACK ([12]).

Let us first take $\alpha = 1$. We assess the adaptive `Algorithm 5.1` starting from a uniform initial mesh consisting of 4226 elements. We fix a maximum number of iterations equal to 10 and choose a global tolerance equal to 10^{-3}.
Figure 3 (top-left) and 4 (top-left) show the second and final adapted grid, respectively, together with two details around the center of the domain (right) and the upper right boundary layer (bottom-left). A comparison of the figures highlights the remarkable difference in the number of triangles: the second adapted

grid has 14785 elements against 7068 of the last adapted mesh. Moreover, in the first case the triangles are more scattered in attempting at capturing all the directional features. On comparing these features with c_0 in Figure 2 (right), we may notice a grid refinement also in areas not meaningful for c_0. Actually, this can be justified by the plot in Figure 5 (right), i.e., by the behaviour of the adjoint state variable λ. This sounds consistent with the spirit of the goal-oriented approach and with the idea leading to our adaptive procedure which merges the information coming from the state, the adjoint state and the gradient equation according to (35). Notice that the contribution of the control variable in (35) via the term $\left(\overline{\mathcal{R}}_K^q\right)^2 \overline{G}_K^*(q)$ vanishes as $\overline{\mathcal{R}}_K^q = 0$ due to the gradient equation $(5)_3$.
Figure 5 (left) displays the state variable obtained on the last adapted mesh. The mismatch with respect to the observation c_0 in Figure 2 is justified by the relatively large value assumed for the Tikhonov regularization parameter α. As expected, a reduction of this value down to 10^{-4} allows us to obtain a state variable closer to c_0 (see Figure 8, left).
Keeping the value $\alpha = 10^{-4}$, and still employing 10 maximum iterations and a global tolerance 10^{-3}, we obtain the grids in Figure 6 (top-left) and 7 (top-left), at the third and last iteration, respectively. It is apparent the absence of the adjoint state contribution in this case. This finds a justification in Figure 8 (right) which represents λ on the tenth adapted grid and clearly stresses its smallness. On comparing both the corresponding whole meshes and the two zooms, we appreciate the more anisotropic nature of the final adapted grid.

6.2 An environmental application

In this section we focus on a test case of some environmental interest. In particular, we study the diffusion and the transport of a certain pollutant emitted by industrial chimneys in the presence of a strong wind. The goal is to measure the concentration of such a pollutant in an observation area, e.g., a town, and consequently to keep it below a given attention level by suitably regulating the chimneys emission.
This aim is similar to the one pursued in Section 4.2 in [14], but cast in an anisotropic framework. The employment of an anisotropic setting is justified by the evident directional features induced by the strong advective field (wind).
Under reasonable assumptions the phenomena at hand can be modeled via the 2D linear scalar advection-diffusion-reaction equation in (1) (see, e.g., [17]). The main assumptions behind this model can be thus summarized:

- the diffusion and transport of the pollutant is tracked on a $x_1 - x_2$ plane parallel to soil at an effective height H coinciding with the mean cross-section of the emitted plumes;

- air motion is described by a medium wind field plus additional terms modeling the turbulent diffusion. With reference to $(1)_1$, $\boldsymbol{\beta}$ takes into account

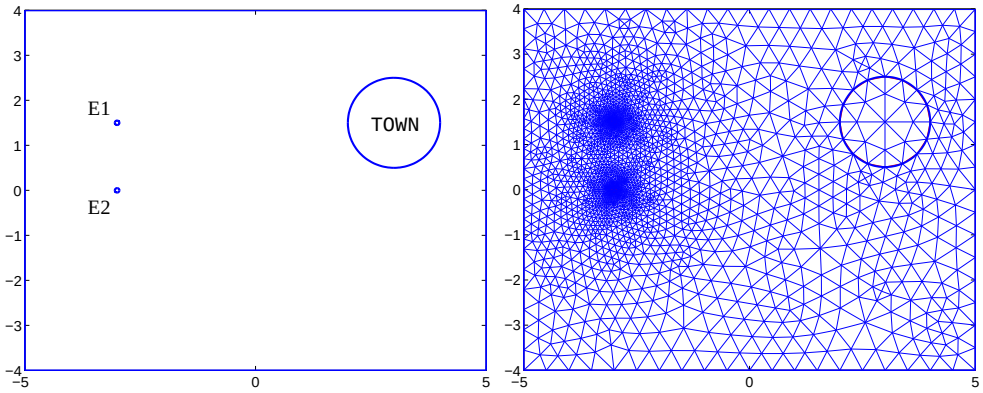

Figure 9: Reference configuration for the two-chimney test case (left) and initial mesh (right).

the medium wind field, while the turbulent diffusion is represented by the function ε. The molecular diffusion is thus neglected;

- the 3D concentration of the plumes follows the Gaussian model $u(x_1, x_2, x_3) = P(x_1, x_2, x_3)\, u(x_1, x_2)$, where

$$P(x_1, x_2, x_3) = \exp\Big(-\frac{1}{2}\Big[\frac{x_3 - H}{\sigma_3}\Big]^2\Big) + \exp\Big(-\frac{1}{2}\Big[\frac{x_3 + H}{\sigma_3}\Big]^2\Big)$$

models the vertical distribution along the x_3 axis and the reflection from the soil, and $\sigma_3 = \sigma_3(x_1, x_2)$ represents the vertical dispersion coefficient depending on the atmospheric stability class and soil orography ([17]). Our interest is for neutral atmospheric conditions in the presence of rural and urban soil;

- in the urban scale approximation, the reaction term can be neglected.

Let us describe the environmental configuration under investigation (see Figure 9 (left)). We identify the computational domain Ω with the rectangle $(-5, 5) \times (-4, 4)$ km. We are tracking the sulfur dioxide (SO_2) concentration associated with two emitting chimneys, both characterized by an effective height $H = 100$ m. A maximum emission rate $\mathcal{F} = 800$ gs^{-1} is assumed for the two chimneys, inducing a maximum emission density $q_{max} = \mathcal{F}\sigma_3^{-1}\sigma_{12}^{-2}$ gs^{-1}m^{-3}, σ_{12} being the horizontal dispersion coefficient. Notice that in the definition of q_{max} both σ_{12} and σ_3 are evaluated at $r = 2000$ m. The emission areas $E1$ and $E2$ are then modeled by two circular regions centered at $(-3, 0)$, $(-3, 1.5)$ km, respectively, both with radius equal to 50 m (see Figure 9 (left)), the emission density being here assumed constant. The expression adopted for σ_{12} and σ_3 is

$$\sigma_{12} = 0.12\, r\, (1 + 0.00025\, r)^{-0.5}\text{m}, \quad \sigma_3 = 0.04\, r\, (1 + 0.0002\, r)^{-0.5}\text{m} \qquad (40)$$

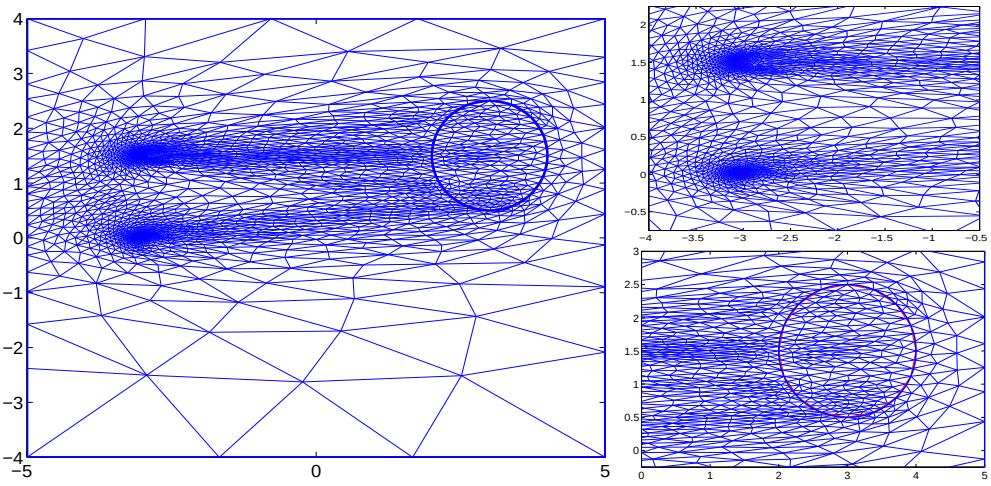

Figure 10: Sixth adapted grid for the two-chimney test case: global grid (left); a zoom around the chimneys (top-right) and the town (bottom-right).

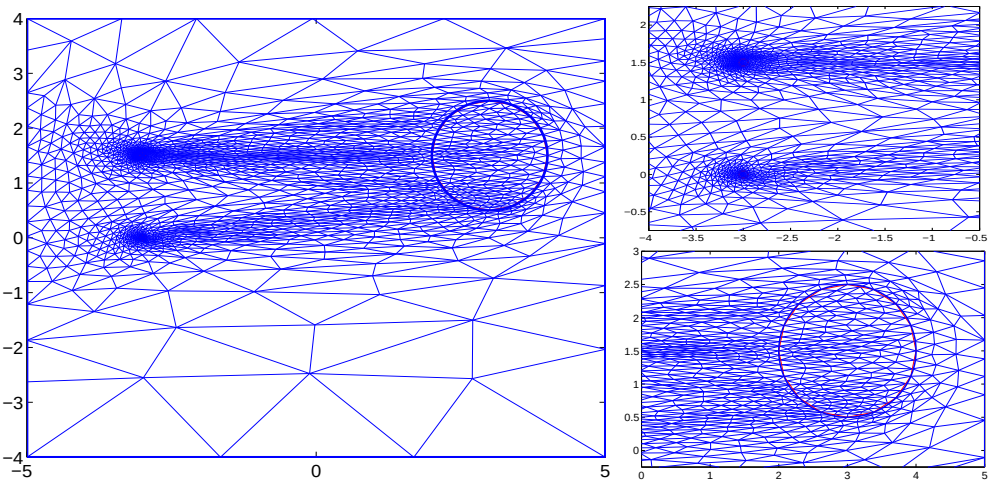

Figure 11: Final adapted grid for the two-chimney test case: global grid (left); a zoom around the chimneys (top-right) and the town (bottom-right).

according to the hypotheses advanced for the atmospheric conditions and the orography. The variable r in (40) measures the (common) horizontal component of the distance of any point in Ω from either the emission sources, i.e., $r = \max(1000\,|x_1 + 3|, 100)$ m. The max avoids the vanishing of r at $x_1 = -3$.

With reference to the model problem (1), we complete the specification of the data by choosing: $\boldsymbol{\beta} = (W, 0)^T$, with $W = 2.5$ ms^{-1}; $\varepsilon = \sigma_{12}^2\, W\, (2r)^{-1}$; $f = 0$; finally the control q plays the role of the emission density in gs^{-1}m^{-3}.

Concerning the boundary conditions, we assign homogeneous Neumann data except on the boundary $\{(x_1, x_2) : x_1 = -5\,\mathrm{km}, -4 < x_2 < 4\,\mathrm{km}\}$, where a homogeneous Dirichlet condition holds. The Neumann data can be incorporated in the a posteriori analysis of section 4 in a straightforward way. In more detail, it suffices to suitably redefine the boundary state and adjoint state residuals in (19) and (21).
Moving to the control framework, since we are interested in monitoring the SO_2 concentration over the urban area `TOWN` in Figure 9 (left), we have to suitably modify the definition of the cost functional in (3). In particular we take

$$J(u, q) = J(u) = \frac{1}{2} \int_{\mathtt{TOWN}} (cu - c_0)^2 \, d\,\mathtt{TOWN},$$

where the observation c_0 represents the attention level fixed to 150 $\mu\mathrm{gm}^{-3}$; the observation operator c coincides with the projection to the soil $P(x_1, x_2, 0) = 2\exp\big(-0.5\,H^2\,\sigma_3^{-2}\big)$. Notice that the Tikhonov regularization parameter is neglected in this case.
The observation space H coincides with $L^2(\mathtt{TOWN})$, while Q reduces to $\mathbb{R}^2$. This latter definition simplifies the optimal control problem: we are led to work in a finite dimensional framework ($\mathbb{R}^2$) so that the discrete problem (6)-(8) is solved by the Newton method in one iteration.

Figures (10) (left) and (11) (left) gather the sixth and the tenth adapted grids yielded by `Algorithm 5.1` by selecting a global tolerance equal to 10^3 and for a maximum number of 10 iterations. Notice that the choice of the global tolerance is consistent with the expected value for J, of about 6000 $(\mu\mathrm{gm}^{-3})^2$ km^2. The modest grid refinement of the two grids upwind the chimneys pertains to the goal-oriented effect. As appreciable in Figure 12 (bottom-right), the adjoint state problem detects the regions mostly influencing the cost functional J, including the zone behind the chimneys. Moreover, the adjoint state solution exhibits a strong boundary layer across the Dirichlet boundary. We remark also that the Gaussian model is not suited for describing the phenomenon upwind the emitting sources.
The two details in Figures 10 (right) and 11 (right) zoom in on the areas around the chimneys and the town. They both highlight the strong anisotropic features of the adapted meshes, detected in a slightly clear-cut way on the last grid. The number of mesh elements is 3903 versus 3322 in the two cases, respectively.

The optimal values returned by the adaptive procedure at the last iteration are $q_1 = 0.155\,q_{max}$ $\mathrm{gs}^{-1}\mathrm{m}^{-3}$ and $q_2 = 0.402\,q_{max}$ $\mathrm{gs}^{-1}\mathrm{m}^{-3}$ for the two emissions in $E1$ and $E2$, respectively. This suggests that, in order to keep the SO_2 concentration below the attention level, the first chimney has to operate about at 15.5% of its full power, while $E2$ is allowed to work at a greater power, of about 40% of its maximum capacity. The corresponding minimum and maximum SO_2 concentration values over the town are 3.42 and 150.5 $\mu\mathrm{gm}^{-3}$. This corroborates the real effectiveness of the resulting control policy.

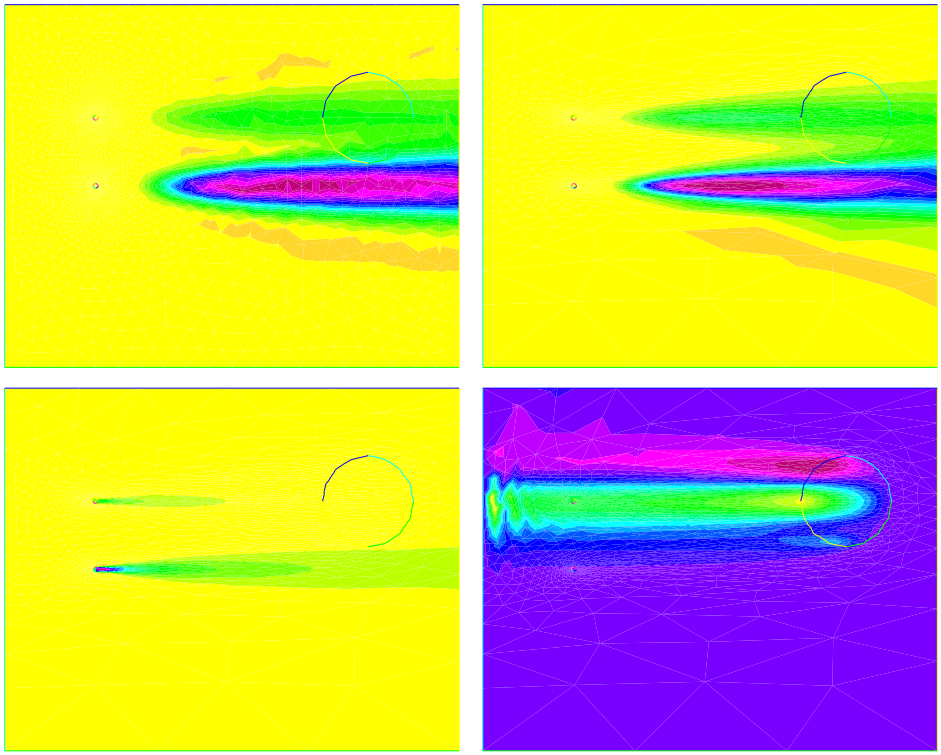

Figure 12: SO_2 concentration at soil on the initial (top-left) and last adapted (top-right) grid; SO_2 concentration at the effective height H (bottom-left) and adjoint state solution (bottom-right) on the last adapted grid.

The different emission density distribution of the two chimneys finds a confirmation in Figure 12. The two plots on top display the SO_2 concentration at soil computed on the initial (left) and on the last adapted (right) grid, while the bottom-left plot shows the same quantity at the effective height on the last adapted mesh. It is clear that $E2$ has a greater power. The improvement brought by the adaptive procedure is corroborated by the higher sharpness of the contour lines. The adjoint state variable in Figure 12 (bottom-right) lets $E2$ be more free to emit at a larger extent, $E2$ being at the side of the influence area of λ.

7 Conclusions

The proposed anisotropic mesh adaptation procedure driven by a suitable a posteriori error estimator seems promising in the light of the numerical assessment performed in section 6. This work represents the first step towards a broader range of validations. Also a more thorough quantitative investigation still needs to be carried out.

Acknowledgment

We thank Prof. Frédéric Hecht for his hints about some implementation issues in `FreeFem++`. We also thank Prof. Boris Vexler for his suggestions about the stabilization scheme.

References

[1] R.A. Bartlett, M. Heinkenschloss, D. Ridzal and B.G. van Bloemen Waanders, *Domain decomposition methods for advection dominated linear-quadratic elliptic optimal control problems*, Comput. Methods Appl. Mech. Engrg., 195 (2006), pp. 6428–6447.

[2] R. Becker, *Mesh adaption for stationary flow control*, J. Math. Fluid Mech., 3 (2001), pp. 317–341.

[3] R. Becker, H. Kapp, and R. Rannacher, *Adaptive finite element methods for optimal control of partial differential equations: basic concept*, SIAM J. Control Optim., 39 (2000), pp. 113–132.

[4] R. Becker and R. Rannacher, *An optimal control approach to a posteriori error estimation in finite element methods*, Acta Numer., 10 (2001), pp. 1–102.

[5] R. Becker and B. Vexler, *Optimal control of the convection-diffusion equation using stabilized finite element methods*, Numer. Math., 106 (2007), pp. 349-367.

[6] F. Brezzi and M. Fortin, *Mixed and Hybrid Finite Element Methods*, Springer-Verlag, New York, 1991.

[7] E. Burman and P. Hansbo, *Edge stabilization for Galerkin approximations of convection-diffusion-reaction problems*, Comput. Methods Appl. Mech. Engrg., 193 (2004), pp. 1437–1453.

[8] E. Burman, M.A. Fernández and P. Hansbo *Continuous interior penalty finite element method for Oseen's equations*, SIAM J. Numer. Anal., 44 (2006), pp. 1248–1274.

[9] Ph. Ciarlet, *The Finite Element Method for Elliptic Problems*, North-Holland Publishing Company, Amsterdam, 1978.

[10] Ph. Clément, *Approximation by finite element functions using local regularization*, RAIRO Anal. Numér., 2 (1975), pp. 77–84.

[11] S.S. Collis and M. Heinkenschloss, *Analysis of the streamline upwind Petrov Galerkin method applied to the solution of optimal control*

problems, Technical Report TR02-01, Department of Computational and Applied Mathematics, Rice University, Houston, TX 77005-1892, 2002 (`http://www.caam.rice.edu/~heinken/papers/supg_analysis.html`).

[12] T.A. Davis, *Users' Guide for the Unsymmetric-pattern MultiFrontal Package (UMFPACK)*, Version 1.1, 1993 (`http://www.cise.ufl.edu/research/sparse/umfpack/`).

[13] L. Dedè, S. Micheletti and S. Perotto, *Anisotropic error control for environmental applications*, accepted for the publication in Appl. Numer. Math., (2008), doi:10.1016/j.apnum.2007.07.008.

[14] L. Dedè and A. Quarteroni, *Optimal control and numerical adaptivity for advection-diffusion equations*, M2AN Math. Model. Numer. Anal., 39 (2005), pp. 1019–1040.

[15] J. Douglas and T. Dupont, *Interior penalty procedures for elliptic and parabolic Galerkin methods*, in R. Glowinski, J.L. Lions (Eds.), Computing Methods in Applied Sciences, Springer-Verlag, Berlin, 1976.

[16] E. Fernández-Cara and E. Zuazua, *Control theory: history, mathematical achievements and perspectives*, Boletin SEMA, 26 (2003), pp. 79–140.

[17] G. Finzi, M. Pirovano and M. Volta, *Gestione della Qualità dell'Aria. Modelli di Simulazione e Previsione*, Mc Graw–Hill, Milano, 2001.

[18] L. Formaggia, S. Micheletti and S. Perotto, *Anisotropic mesh adaptation in Computational Fluid Dynamics: application to the advection-diffusion-reaction and the Stokes problems*, Appl. Numer. Math., 51 (2004), pp. 511–533.

[19] L. Formaggia and S. Perotto, *New anisotropic a priori error estimates*, Numer. Math., 89 (2001), pp. 641–667.

[20] L. Formaggia and S. Perotto, *Anisotropic error estimates for elliptic problems*, Numer. Math., 94 (2003), pp. 67–92.

[21] P.-L. George and H. Borouchaki, *Delaunay Triangulation and Meshing. Application to Finite Elements*, Editions Hermés, 1998.

[22] M.B. Giles and E. Süli, *Adjoint methods for PDEs: a posteriori error analysis and postprocessing by duality*, Acta Numer, 11 (2002), pp. 145–236.

[23] F. Hecht, O. Pironneau and A. Le Hyaric, *FreeFem++ Manual*, Version 2.24-3, 2008 (`http://www.freefem.org/ff++`).

[24] J.L. Lions, *Optimal Control of Systems Governed by Partial Differential Equations*, in Grundlehren Math. Wiss, Volume 170, Springer, Berlin, 1971.

[25] J.L. Lions and E. Magenes, *Non-Homogeneous Boundary Value Problems and Applications*, Volume I, Springer-Verlag, Berlin, 1972.

[26] Y. Maday and A.T. Patera, *Numerical analysis of a posteriori finite element bounds for linear functional outputs*, Math. Models Methods Appl. Sci., 10 (2000), pp. 785–799.

[27] S. Micheletti, S. Perotto, and M. Picasso, *Stabilized finite elements on anisotropic meshes: a priori error estimates for the advection-diffusion and Stokes problems*, SIAM J. Numer. Anal., 41 (2003), pp. 1131–1162.

[28] S. Micheletti and S. Perotto, *Reliability and efficiency of an anisotropic Zienkiewicz–Zhu error estimator*, Comput. Methods Appl. Mech. Engrg., 195 (2006), pp. 799–835.

[29] S. Micheletti and S. Perotto, *Output functional control for nonlinear equations driven by anisotropic mesh adaption. The Navier-Stokes equations*, accepted in SIAM J. Sci. Comput., (2008).

[30] J.T. Oden and S. Prudhomme, *Goal-oriented error estimation and adaptivity for the finite element method*, Comput. Math. Appl., 41 (2001), pp. 735–756.

[31] J.T. Oden and J.N. Reddy, *Variational Methods in Theoretical Mechanics*, 2nd ed., Springer, Berlin and Heidelberg, 1983.

[32] M. Picasso, *Anisotropic a posteriori error estimate for an optimal control problem governed by the heat equation*, Numer. Methods Partial Differential Equations, 22 (2006), pp. 1314–1336.

[33] R. Rodriguez, *Some remark on the Zienkiewicz–Zhu estimator*, Numer. Methods Partial Differential Equations, 10 (1994), pp. 625–635.

[34] V. Thomée, *Galerkin Finite Element Methods for Parabolic Problems*, Springer Series in Computational Mathematics, Vol. 25., 2nd edn, Springer-Verlag, Berlin, 2006.

[35] B. Vexler, *private communication*, 2008.

[36] O.C. Zienkiewicz and J.Z. Zhu, *A simple error estimator and adaptive procedure for practical engineering analysis*, Internat. J. Numer. Methods Engrg., 24 (1987), pp. 337–357.

[37] O.C. Zienkiewicz and J.Z. Zhu, *The superconvergent patch recovery and a posteriori error estimates. Part 1: the recovery technique*, Internat. J. Numer. Methods Engrg., 33 (1992), pp. 1331–1364.

MOX Technical Reports, last issues

Dipartimento di Matematica "F. Brioschi",
Politecnico di Milano, Via Bonardi 9 - 20133 Milano (Italy)

15/2008 S. Micheletti, S. Perotto:
An anisotropic mesh adaptation procedure for an optimal control problem of the advection-diffusion-reaction equation

14/2008 C. D'Angelo, P. Zunino:
A finite element method based on weighted interior penalties for heterogeneous incompressible flows

13/2008 L.M. Sangalli, P. Secchi, S. Vantini, V. Vitelli:
K-means alignment for curve clustering

12/2008 T. Passerini, M.R. de Luca, L. Formaggia, A. Quarteroni, A. Veneziani:
A 3D/1D geometrical multiscale model of cerebral vasculature

11/2008 L. Gerardo Giorda, L. Mirabella, F. Nobile, M. Perego, A. Veneziani:
A model preconditioner for the Bidomain problem in electrocardiology

10/2008 N. Grieco, E. Corrada, G. Sesana, G. Fontana, F. Lombardi, F. Ieva, A.M. Paganoni, M. Marzegalli:
Predictors of the reduction of treatment time for ST-segment elevation myocardial infarction in a complex urban reality. The MoMi^2 survey

9/2008 P. Secchi, E. Zio, F. Di Maio:
Quantifying Uncertainties in the Estimation of Safety Parameters by Using Bootstrapped Artificial Neural Networks

8/2008 S. Micheletti, S. Perotto:
Space-time adaptation for purely diffusion problems in an anisotropic framework

7/2008 C. Vergara, R. Ponzini, A. Veneziani, A. Redaelli, D. Neglia, O. Parodi:
Reliable CFD-based Estimation of Flow Rate in Hemodynamics Measures. Part II: Sensitivity Analysis and First Clinical Application

6/2008 E. Fumagalli, L. Lo Schiavo, A.M. Paganoni, P. Secchi:
Statistical analyses of exceptional events: the Italian experience